Research Article

Sanmun Kim, Jeong Min Shin, Jaeho Lee, Chanhyung Park, Songju Lee, Juho Park, Dongjin Seo, Sehong Park, Chan Y. Park and Min Seok Jang*

Inverse design of organic light-emitting diode structure based on deep neural networks

https://doi.org/10.1515/nanoph-2021-0434
Received August 9, 2021; accepted October 19, 2021;
published online November 4, 2021

Abstract: The optical properties of thin-film light emitting diodes (LEDs) are strongly dependent on their structures due to light interference inside the devices. However, the complexity of the design space grows exponentially with the number of design parameters, making it challenging to optimize the optical properties of multilayer LEDs with rigorous electromagnetic simulations. In this work, we demonstrate an artificial neural network that can predict the light extraction efficiency of an organic LED structure in 30 ms, which is ~10^3 times faster than the rigorous simulation in a single-treaded execution with root-mean-squared error of 1.86×10^{-3}. The effective inference time per structure is brought down to ~0.6 μs with unaltered error rate with parallelization. We also show that our neural networks can efficiently solve the inverse problem – finding a device design that exhibits the desired light extraction spectrum – within the similar time scale. We investigate the one-to-many mapping issue of the inverse problem and find that the degeneracy can be lifted by incorporating additional emission spectra at different observing angles. Furthermore, the forward neural network is combined with a conventional genetic algorithm to address additional large-scale optimization problems including maximization of light extraction efficiency and minimization of angle dependent color shift. Our approach establishes a platform for tackling computation-heavy optimization tasks with one-time computational cost.

Keywords: deep neural network; genetic algorithm; inverse design; light extraction efficiency; organic light-emitting diodes.

***Corresponding author: Min Seok Jang**, School of Electrical Engineering, Korea Advanced Institute of Science and Technology, Daejeon 34141, Republic of Korea, E-mail: jang.minseok@kaist.ac.kr. https://orcid.org/0000-0002-5683-1925
Sanmun Kim, Jeong Min Shin, Jaeho Lee, Chanhyung Park, Songju Lee and Juho Park, School of Electrical Engineering, Korea Advanced Institute of Science and Technology, Daejeon 34141, Republic of Korea
Dongjin Seo, School of Electrical Engineering, Korea Advanced Institute of Science and Technology, Daejeon 34141, Republic of Korea; and KC Machine Learning Lab, Seoul 06181, Republic of Korea
Sehong Park, OC Optical Technology Task, LG Display, Seoul, 07796, Republic of Korea
Chan Y. Park, KC Machine Learning Lab, Seoul 06181, Republic of Korea

1 Introduction

Organic light-emitting diodes (OLED) are widely used light-emitting diodes that utilize the light emission from an electron-hole annihilation inside an organic material [1]. Unique advantages that come from tailored structures of OLED devices such as high power efficiency, high color purity, ability to express true black state, the feasibility of creating a light-weight device, and its potential flexibility propelled them to a huge demand in lighting and displays [2–8].

Multiple reflections and light interferences inside a layered OLED cause its optical characteristics to depend heavily on the device shape; even with the same materials, the light emission efficiencies and spectral characteristics can be dramatically varied [9, 10]. Also, it leads to an angular dependence of the emission spectra while narrowing down the emission spectra. In this manner, an optimization process is required for any OLED device for the maximization of light extraction efficiency and color gamut. Some classical approaches have been made to optimize the structure but the results are rarely globally optimal since the global optimization requires heavy computation [10–12].

In the meantime, it has been reported that neural networks work as an excellent platform for calculating the optical responses of a photonics device. Multiple inverse design problems have been tackled with the aid of machine learning [13–17]. Some researchers accomplished inverse design with the backpropagation method where the error in the final network is propagated back to correct the inputs

[18, 19]. Also, generative models such as generative adversarial networks (GAN) have been applied to the inverse design of a metasurface structure [20–22]. Amongst them, Global optimization based on generative neural networks (GLOnet) proved itself to be data-efficient than other generative models by utilizing the physical value for loss function calculation [23]. Other networks including recurrent neural network [24], variational auto-encoder [25] have also been applied for the inverse design and proved their possibilities.

Machine learning techniques have been performed to improve the OLED performance in multiple directions. The random forest algorithm has been employed to extract the underlying correlations in the design of blue phosphorescent OLED [26], revealing triple energy of the electron transport layer to be the most critical parameter. Also, a virtual screening through machine learning has been applied to select the molecules for OLED from a pool of 1.6 million candidates [27]. Time-difference density functional theory calculation results of 40,000 molecules were used as a training set and calculation results from selected molecules were added to the dataset during the training. However, no attempt has been made to address the link between the device design parameters and the light extraction efficiency (LEE) of a given OLED device for the purpose of inverse design and optical performance optimization.

In this work, we present a deep learning-based design scheme that can efficiently solve large-scale OLED optical performance optimization problems. We first develop an artificial neural network that receives the layer thicknesses and refractive indices of an OLED structure as the inputs and predicts its LEE spectrum with a marginal error. We then show that an artificial neural network can also be trained to solve the inverse problem instantly: finding an OLED structure exhibiting a given LEE spectrum. We address the central physical problem of inverse scattering – the one-to-many mapping issue – by investigating how the inverse-designed device parameters are related to the original design parameters and demonstrate that it is possible to lift the degeneracy and determine design parameters uniquely from the optical properties by incorporating multiple emission spectra collected from different observing angles. Finally, we combine the forward network with a genetic algorithm to tackle additional OLED optimization problems including maximization of light extraction efficiency and minimization of angular color shift. The results of these large-scale optimization problems provide interesting physical insights that can be potentially generalized in designing OLED devices. The neural network-based design scheme provides a promising platform to address large design spaces that cannot be handled by conventional numerical approaches based on rigorous simulations.

2 Results and discussion

2.1 OLED structure and light extraction efficiency

In this work, we use a simplified structure of a generic OLED defined by six parameters as shown in Figure 1a. The topmost layer is set as an infinitely thick polyacrylate layer, considering the fact that light can penetrate the polyacrylate-air

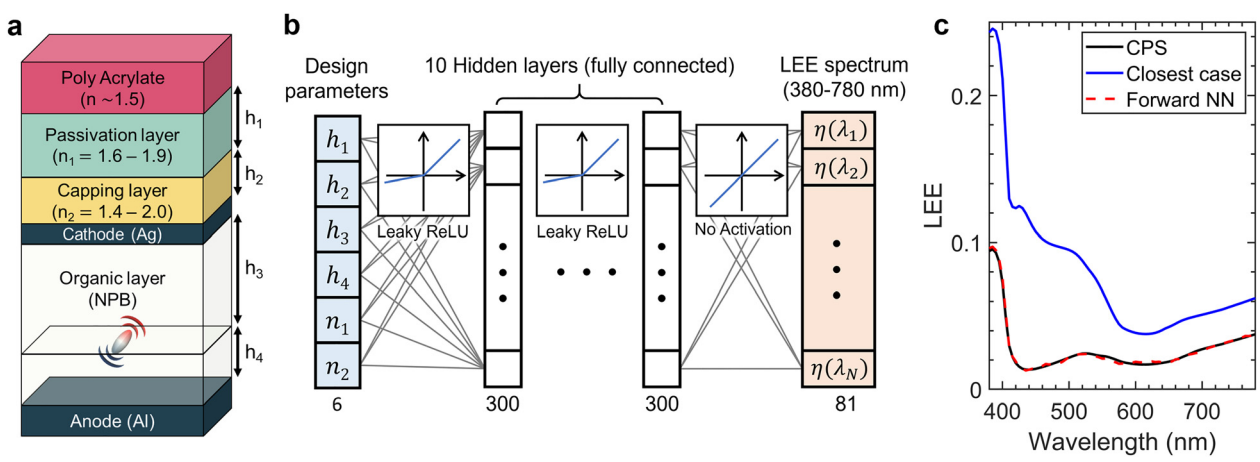

Figure 1: Forward prediction of light extraction efficiency of an OLED strucutre.
(a) A schematic of simplified top-emitting OLED structure used in this work. (b) A diagram of the forward neural network structure. Ten hidden layers, each with 300 nodes constitute the neural network. Leaky rectified linear activation (Leaky ReLU) function is used as activation functions except for the last layer where no activation function is applied. (c) The LEE curve calculated from the CPS model (black), forward neural network (red, dashed). The LEE curve of the closest sample in design parameter space is plotted together (blue). The design parameters (h_1, h_2, h_3, h_4, n_1, n_2), were (725, 136, 12, 240 nm, 1.80, 1.52) for CPS and forward neural network, and (693, 138, 24, 227 nm, 1.80, 1.49) for the closest case.

boundary with negligible loss by the application of anti-reflection coating. The polyacrylate layer is followed by the passivation and the capping layer, each with a non-dispersive constant refractive index n_1 and n_2 and thickness h_1 and h_2, respectively. The device is assumed to have an Al bottom anode and a 12 nm thick Ag top cathode. Since most organic semiconductors have refractive indices near 1.75, the organic layers between the electrodes are modeled with a single N,N′-Di(1-naphthyl)-N,N′-diphenyl-(1,1′-biphenyl)-4,4′-diamine (NPB) layer [28]. The thickness of the organic layer is set as $h_3 + h_4$ with light emission occurring at a distance h_4 above the anode. To account for the parasitic absorption and to enhance the numerical stability, a small loss is introduced to the organic layer (except for the emitting medium) and the capping layer by setting the imaginary parts of their refractive indices being 1/1000 of their real parts (Section S1 of Supplementary Material).

Light extraction efficiency (LEE), $\eta(\lambda)$, of an OLED is defined as the ratio of the light power leaving the device to the net power dissipation by dipoles at a wavelength λ. Conventionally, LEE is rigorously calculated by decomposing the emission from a dipole inside the emission layer into plane waves according to their wavevector and tracking their propagation inside the device using the transfer matrix method. This method, called the Chance–Prock–Silbey (CPS) model [29], is utilized here to create the dataset for the training of the forward neural network and to provide the ground truth to check the validity of the trained network. For our work, a randomly sampled dataset containing 260,000 OLED design-LEE spectra pair was created. Although neural networks can be trained with a far smaller number of samples as illustrated in Figure S2a, a larger training set was employed for the sake of prediction accuracy.

2.2 Forward neural network

We first train a neural network that can predict the LEE spectrum of a given device structure. The detailed network structure is illustrated in Figure 1b. The inputs of the neural network have six parameters: the refractive index and the thickness of the passivation (n_1, h_1) and capping (n_2, h_2) layer, and the distance of the emissive plane from the cathode (h_3) and anode (h_4). Considering the fabrication feasibility, the domain of each parameters is set to $n_1 = 1.6$–1.9, $n_2 = 1.4$–2.0, $h_1 = 500$–1500 nm, and $h_{2-4} = 10$–250 nm. The input variables are normalized to have values between 0 and 1 to remove the bias arising from input parameter distribution. The outputs of the neural network are LEE $\eta(\lambda)$ spectra evaluated at 81 equally spaced wavelength points between $\lambda = 380$–780 nm, which covers the entire visible range. The neural network for the forward prediction has 10 hidden layers and each layer is equipped with 300 nodes. The corresponding number of trainable parameters/weights is 838,581, which is huge compared to other spectrum prediction networks [18, 19, 30]. This design is adopted since the prediction accuracy is our major interest and the prediction error monotonically decreases as the network complexity escalates as shown in Figure S2b, c. The monotonicity is likely due to CPS calculations having only a negligible error and thus leading to minimal over-fitting. As the activation function, a leaky rectified linear unit (leaky-ReLU) is employed to circumvent the vanishing gradient problem, which may occur when an inverse neural network is added to the anterior part, forming an 18-layer-deep network.

After 5000 training epochs with 260,000 training samples (Figure S3), the trained forward network successfully infers the LEE spectrum as shown in Figure 1c. The root-mean-square error (RMSE) is 1.86×10^{-3}, which is small enough for the inverse design and device optimization applications. We note that, in the example shown in Figure 1c, the closest sample in the training set, chosen to have the closest normalized input parameters to those of the target device, still shows a significant deviation from the accurate spectrum. This exemplifies that the problem of predicting LEE from the device parameters is not a trivial task even with a large number of training data, justifying the necessity of a large neural network and also demonstrating that the neural network does not just memorize the training data.

The prediction error increases rapidly as the input variables leave the trained range. As shown in Figure S4, a seven-fold increase in RMSE is observed (1.30×10^{-2}) when h_3 or h_4 deviates from the trained domain by 10%. The limited extrapolation capability implies that the forward neural network has not learned the underlying physics from the training process but only learned to predict LEE by interpolating from the preexisting dataset. The extrapolation capability of the neural network is expected to improve if the degree of overfitting is lowered by reducing the network complexity.

The inference time of the forward neural network for a given OLED structure is about 30 ms in a single-threaded CPU execution, which is ~10^3 times faster than the rigorous CPS calculation in a similar condition. The neural network calculation can be readily parallelized using a GPU. We found that, with NVIDIA® Tesla® V100 GPU accelerator, the parallelized inference process takes ~600 ms when 10^6 structures, characterized by six design parameters, are simultaneously fed to the neural network, and thus the effective inference time per structure is brought down to ~0.6 μs. Hence, the computation time is dominated by the

time spent on data creation and neural network training, which took ~7 days and ~1 h, respectively (in the data creation stage, multiple structures were simulated in parallel using two Intel® Xeon® Gold 5220 processors so the effective calculation time is brought down to 2.4 s). This, however, can be considered as an one-time computational cost (Supplementary Material Section S5), and an optimization involving a neural network performs superior in terms of speed if the total number of candidates considered is greater than the number of datasets required for network training. Also, the supremacy becomes more evident if multiple optimization tasks can be carried out on a single network, as will be presented in this work.

2.3 Inverse neural network

We then tackle the problem of inverse design. Here the neural network is designed to obtain the device parameters from a given LEE spectrum. This problem, however, suffers from the common inverse scattering issue: identical electromagnetic response found in multiple structures. This one-to-many mapping characteristic of the inverse scattering problem causes difficulties in defining the training loss if the output of the neural network is the structure parameters. To circumvent this obstacle, we attach the pretrained forward LEE prediction network with fixed weights after the inverse network as schematically shown in Figure 2b, as suggested in previous works [30, 31]. In this tandem configuration, the training of the network is done by defining the loss as the discrepancy between the input and output LEE spectrum. The last layer before the transferred network adopts a sigmoid as the activation function to regularize the inputs of the latter part of the network to range between 0 and 1.

With the new training scheme, the inverse network was successfully trained by using 260,000 samples, finding a set of OLED design parameters (n_{1-2}, h_{1-4}) exhibiting a LEE spectrum that is nearly identical to the input spectrum within a few milliseconds as shown in Figure 2a. The resulting RMSE of the inverse network is 4.42×10^{-3}. The inverse network consists of eight hidden layers, each equipped with 300 nodes. A neural network with a higher complexity leads to a divergence during the training step and a simpler neural network leads to a greater error.

We note that, since the mapping from an LEE spectrum to device design parameters is inherently one-to-many, the inverse network tends to produce different design parameters that are used to generate the target LEE spectrum as depicted in Figure 2c. One thing to notice in this example is that h_3 and h_4, the thickness of the organic layer above and below the dipole, are well-reproduced by the inverse network, while the other design parameters are largely different. We statistically analyze this tendency by plotting a two-dimensional histogram with the x-axis being the original design parameter used to generate the input LEE spectra and the y-axis being the parameter obtained from the inverse network (Figure S6). As seen in Figure S6c, d, the histograms for h_3 and h_4 are highly peaked on the diagonal line which implies that the original values are preserved by the inverse design. Histograms for all the other parameters still show maxima near the diagonal but

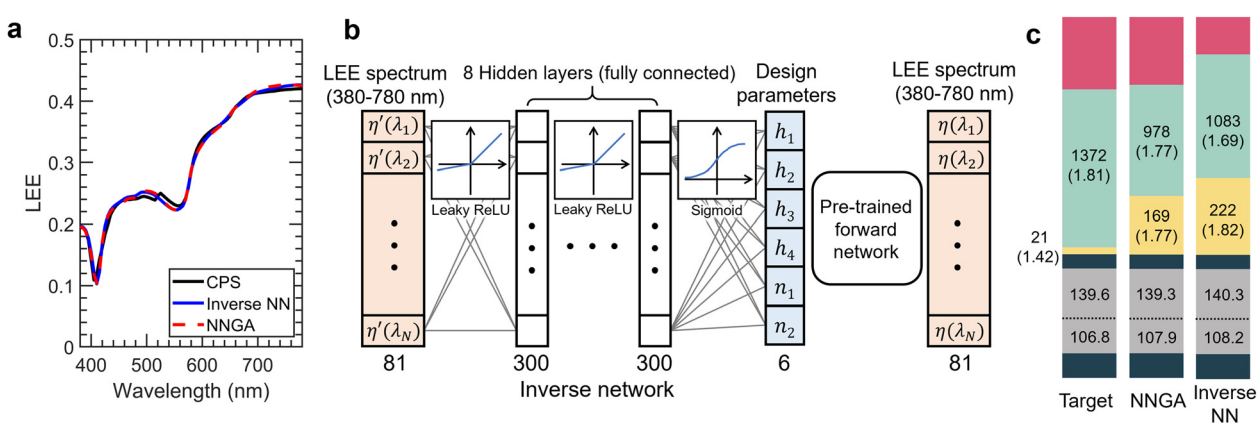

Figure 2: Inverse design of OLED structures based on deep neural networks.
(a) The target LEE curve and the inverse-designed LEE curves from the inverse neural network and NNGA. (b) Schematic of the inverse neural network. The eight-layer-deep neural network was joined before the pretrained spectrum prediction network. (c) Inverse-designed structure parameters. The structure labeled by "Original" corresponds to the design that results in the black solid line of Figure 2a. "NNGA" and "Inverse NN" corresponds to the inverse-designed structure that has LEE values shown as blue solid line and red dashed line in Figure 2a. The number outside the bracket indicates the thickness of the corresponding layer in nanometers and the number inside the bracket is the refractive index of the material. In the figure, the thickness of the passivation layer (green) was shrunk for brevity.

follow their own distributions different from the original ones (Figure S6a, b, e, f). Note that, however, this does not mean that h_3 and h_4 are the only important parameters in determining LEE, as one can easily find the structures that have identical (h_3, h_4) but different (n_1, n_2, h_1, h_2) exhibiting different LEE spectra as illustrated in Figure S6i.

As described above, one-to-many mapping problem is predominant in the inverse design of photonic devices. Since the need of tool for the inverse design of OLED was first suggested for industrial reasons where inferring the actual device structure based on their spectrum is essential, circumventing the inverse scattering issue through tandem network which leads to a completely different design parameters does not resolve the problem. We demonstrate that it is possible to lift the degeneracy and determine the design parameters uniquely from the optical properties by incorporating multiple emission spectra collected from different observing angles (see Supplementary Material S12 for details).

To further analyze the performance of the inverse network, we have also tested if the inverse network can find device designs that correspond to an artificially created LEE spectrum having a constant value $\eta(\lambda) = \eta_0$ over the entire visible range. This task will test the generalizability of the encoder, which may be unfair to the given deep neural network if it hasn't seen such a spectrum during the training step. The resulting RMSE of the inverse-network-based design varies from 0.004 to 0.439 and tends to increase as η_0 increases from 0.01 to 0.6 as illustrated in Figure 3a. Along with this global trend, the RMSE of the inverse-network-based design exhibits an anomalous decrease at around $\eta_0 = 0.25$, which means that the artificial flat LEE spectrum becomes most realizable in our design parameter space at that specific target LEE value. An LEE value higher than 0.5 is rarely obtained in a planar OLED structure and a flat LEE spectrum is impossible to obtain in our problem space. Hence, for $\eta_0 > 0.5$, the error monotonically increases with the target efficiency, η_0.

2.4 Neural network assisted genetic algorithm

Although the inverse neural network successfully designs OLED structures for a target LEE spectrum, many practical design problems require finding a device structure by using a figure of merit (FoM) that cannot be directly translated into the LEE spectrum requirement. To efficiently solve more general design problems, we join the forward prediction network with a genetic algorithm, which mimics the process of natural evolution and has demonstrated high performance from the design of an antenna [32] to the analysis of geothermal heat flux [33]. As the time-consuming rigorous electromagnetic simulation step is replaced by a neural network with ~10^6 times faster calculation speed, the massive optimizations involving 10^9 simulations are enabled to be performed in a reasonable time scale (~10^3 s). The details on how the neural network assisted genetic algorithm (NNGA) work can be found in Section S7 of the Supplementary Material, and a detailed discussion regarding the one-time computational cost of NNGA can be found in Section S5 of Supplementary Material.

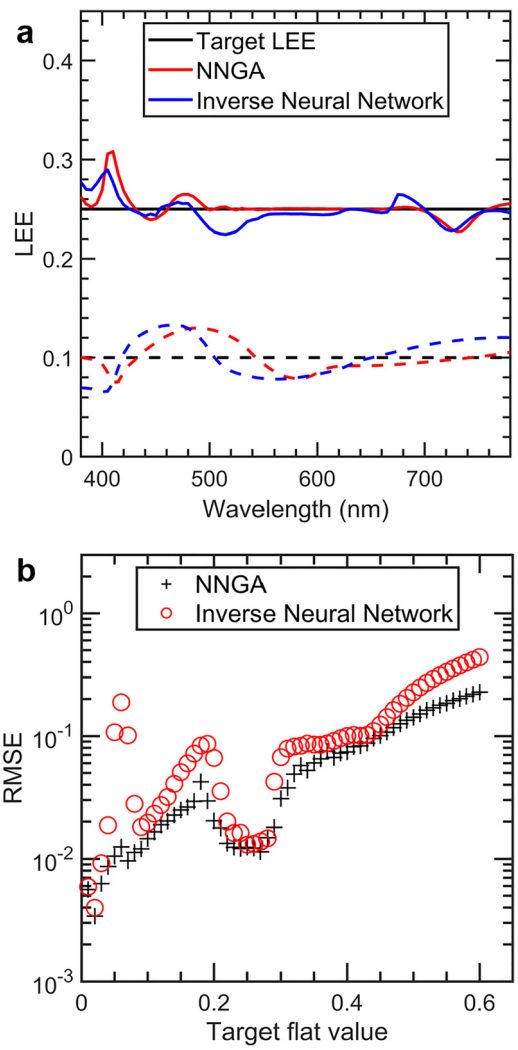

Figure 3: Inverse design of a flat LEE using an inverse neural network and genetic algorithm.
(a) The inverse-designed LEE curve at $\eta_0 = 0.1$ and 0.25. The root-mean-squared error (RMSE) of the inverse neural network and the NNGA was 0.0098, 0.0062 for $\eta_0 = 0.25$ (solid line), and 0.018, 0.011 at $\eta_0 = 0.1$ (dashed line). (b) RMSE value was monitored while changing η_0 from 0.01 to 0.6 with a step size of 0.01. The error tends to increase as the target flat value increases while having a dip near $\eta_0 = 0.25$ for both the NNGA and the inverse neural network. In all cases, the NNGA performed better than the inverse neural network.

We first apply NNGA to the previously described inverse design problems and compare its performance with the inverse neural network. For realistic target LEE spectra, the RMSE of NNGA results is 3.60×10^{-3}, which is smaller than the case of the inverse neural network as illustrated in Figure 2b. For non-existing artificial flat LEE spectra, NNGA produces a better design consistently over all η_0 values as shown in Figure 3a, b. Figure 3b compares the result from NNGA and the inverse network with the target flat LEE spectra with $\eta_0 = 0.01$ and 0.6. To sum up, NNGA generally outperforms the inverse neural network in inverse design problems regardless of whether the target LEE spectra are realistic or artificial, while the time it takes the inverse neural network to provide a set of design parameters (~40 ms) is four orders of magnitude shorter than that of the NNGA (~10^3 s).

As mentioned previously, a wide range of flexibility in defining the loss enables the complex optimization process possible through NNGA. Here, we demonstrate two optimization tasks carried out by NNGA that would otherwise have been impractical due to their heavy computational load when using the CPS method. First, we optimize the OLED structure to maximize its LEE at a given wavelength λ. The optimization for a single wavelength was carried out by performing NNGA with ~100 generations and 65,536 populations in each generation involving ~6×10^7 calculations of LEE. The optimization results for 81 wavelength points (380–780 nm with 5 nm spacing) was summarized in Figure 4. The maximum efficiency is higher than 0.5 for $\lambda > 475$ nm but drops below 0.5 at shorter wavelengths as the index of the organic layer (NPB) increases and thus the light escape cone shrinks. Values of h_3 and h_4 increase as the wavelength increases which is expected as the cathode-organic layer-anode cavity needs to scale with λ. The capping layer index, n_2, almost reaches the upper bound of the design domain ($n_2 \approx 1.97$) possibly to induce a strong cavity effect with large index contrast between the neighboring layers. The thickness of the capping layer thickness, h_2, also increases with λ. Optimized value of h_1 undergoes multiple jumps possibly due to the hopping between different Fabry–Perot cavity conditions (Supplementary Material S9). It should be noted that all results depicted in the plots are not global maxima but only local maxima within our parameter space.

2.5 Minimizing the color shift in white point

Finally, we tackle the problem of an angle-dependent color variation using NNGA. Due to the resonances inside the device, the spectrum of the outcoupled light has an inevitable angular dependence, which causes the well-known issue of color shift depending on viewing angle [34]. In an OLED display, lights from RGB subpixels combine to express the white color (D65 illuminant). By employing NNGA, we optimize OLED structures to have a minimal white color deviation for a wide range of viewing angle ($\theta = 0°$, 15°, 30°, 45°, and 60°). To predict the angular LEE for each viewing angle, five different neural networks were trained with an RMSE of 1.44×10^{-3} sr^{-1} as described in Supplementary Material S9. Here, the white color deviation is defined in CIE 1976 space as $\Delta_{max} = \mathrm{Max}(\Delta_{15}, \Delta_{30}, \Delta_{45}, \Delta_{60})$, where $\Delta_\theta = [(u'_\theta - u'_{D65})^2 + (v'_\theta - v'_{D65})^2]^{1/2}$ and the subpixels are set to display D65 at $\theta = 0°$. Figure 5a illustrates how the subpixels are positioned inside a single pixel. The subpixels are assumed to have Bis(2-methyldibenzo[f,h]quinoxaline)(acetylacetonate)iridium(III) (Ir(MDQ)$_2$acac) [35], Bis(2-phenylpyridine)(acetylacetonate)iridium(III) (Ir(ppy)2acac) [12], and Bis[2-(4,6-difluorophenyl)pyridinato-C2,N](picolinato)iridium (Firpic) [12] emitters for red, green, and

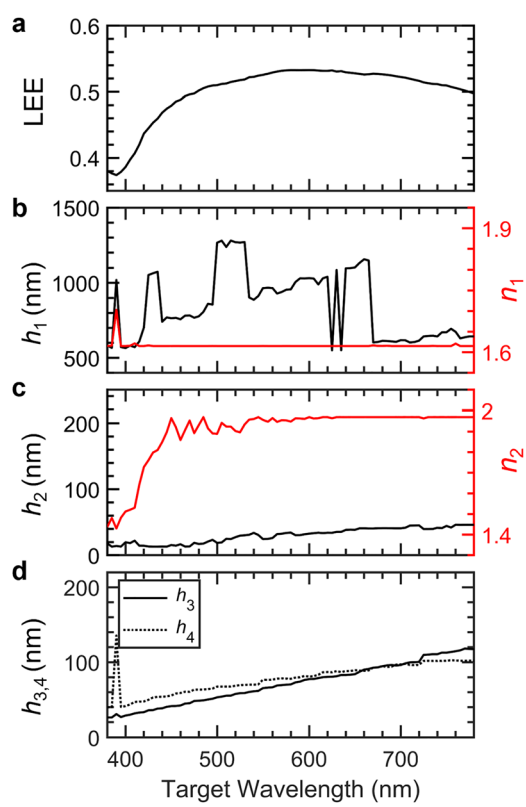

Figure 4: Maximized LEE values and optimal structure parameters of single wavelength dipoles. The curves represent the optimized LEE values and the optimized design parameters of 81 different OLEDs. (a) The maximized LEE values. Thicknesses and refractive indices of (b) the passivation and (c) the capping layer. (d) The thickness of the active layer above and below the dipole.

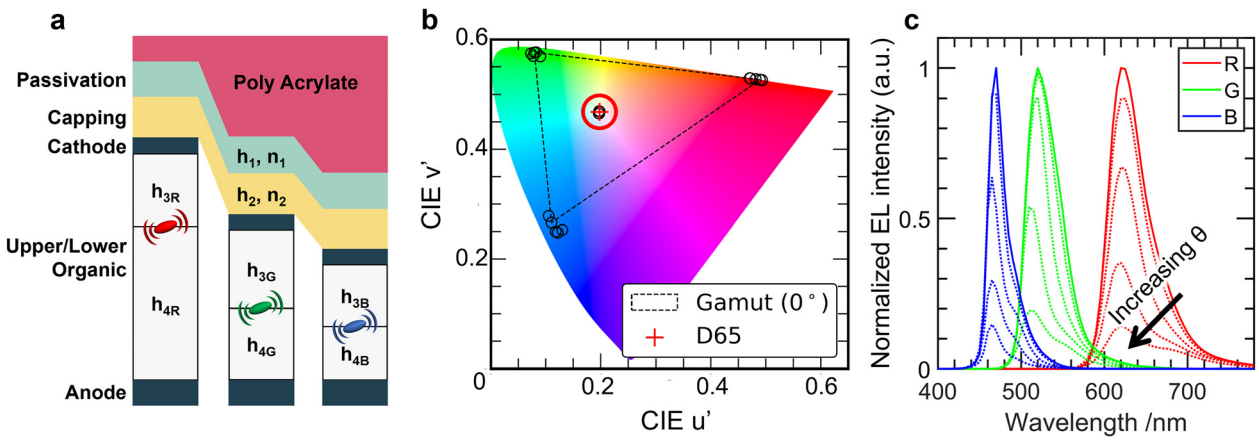

Figure 5: Minimization of the angular color shift in a RGB subpixel OLED.
(a) A schematic of RGB subpixels constituting a pixel in an OLED device. Values of h_{1-2}, and n_{1-2} are shared across the subpixels, resulting in 10 degrees of freedom. The optimized design was (h_1, n_1, h_2, n_2, h_{3R}, h_{4R}, h_{3G}, h_{4G}, h_{3B}, h_{4B}) = (688, 1.77, 80, 1.85, 201, 96, 186, 59, 54, 162 nm). (b) Angle dependent spectra of each subpixel and the white point plotted in CIE 1976 color space. The area surrounded by the dashed line is the color gamut for the observer at 0°. The point marked by a plus mark represents the point of D65 illuminant, the target white. The red circle centered at D65 denotes the set of equidistant points of distance 0.03 from D65 illuminant in CIE 1976 color space. (c) Normalized electroluminescence (EL) spectra of the subpixels. The spectrum at 0° is denoted by the solid line and the spectra at 15°–60° are plotted with dotted lines with spectra generally blue-shifting with the viewing angle. The electroluminescence intensities have been normalized such that the maximum intensity point at 0° viewing angle of R, G, and B spectra are unity [36, 37]. In order to display a white color (D65) with such device, the relative strength of the R/G/B subpixels need to be 1.36: 1: 2.57.

blue, respectively, with independent organic layer thickness configurations $h_{3R,\ 3G,\ 3B}$ and $h_{4R,\ 4G,\ 4B}$, whereas the design parameters for passivation and capping layer, $n_{1,\ 2}$ and $h_{1,\ 2}$, are shared among the subpixels due to the fabrication feasibility. In sum, the problem is to find the optimal design parameters that minimize Δ_{max} in the 10-dimensional design space ($n_{1,\ 2}$, $h_{1,\ 2}$, $h_{3R,\ 3G,\ 3B}$, and $h_{4R,\ 4G,\ 4B}$). The details on the NNGA employed in this section including the information on the additional constraints can be found in section S10 of Supplementary Material.

The optimized device exhibits the maximum white color shift of $\Delta_{max} = 3.3 \times 10^{-3}$ from D65, which is equivalent to 0.83 just noticeable color difference (JNCD) and is below the recognizable limit [12], as presented in Figure 5b. The average LEE weighted with dipole spectrum was 0.325, 0.286, 0.193 for R, G, B subpixels, respectively. The device also has a marginal angular color variation of each subpixel, whose normalized intensity spectra at various angles are provided in Figure 5c. During the optimization, ~2.4×10^6 OLED structures were considered, while the inference time took less than a minute. This task considered color shift as the only optimization target, hence other important factors including luminosity and color gamut may not meet the commercially accepted values. In NNGA, we can always redefine the FoM so that it encompasses the required characteristics.

In real world applications, a typical fabrication process can cause a few percent error in device's thickness, which can impose a significant degradation in the device performance. Robustness from the fabrication error can be considered during the optimization process by adding a Gaussian noise to the design parameters and taking the weighted average of FoMs over the ensemble of structures.

3 Conclusions

The possibility of using a neural network as a platform for the LEE prediction is tested throughout the work. In a single-threaded calculation, the neural network predicting LEE from the OLED design parameters (forward network) is able to complete the calculation in 30 ms, which is ~10^3 times faster than the rigorous electromagnetic simulation based on a CPS formulation with RMSE of 1.86×10^{-3}. The inference time per structure is brought down to ~0.6 μs with an unaltered error rate with GPU parallelization. Two different routes are taken for the inverse design of LEE spectra. One is the inverse neural network built by joining additional layers to the pretrained forward neural network and the other is the NNGA which uses the forward network as the platform for LEE prediction. NNGA shows a superior performance in the inverse design of both existing and nonexisting LEEs whereas the inverse neural network was unmatched in terms of the computation speed. The NNGA also successfully solves two representative OLED optimization problems: maximizing the LEE and minimizing the

angle-dependent white color variation. Considering that both problems possess large design spaces that are difficult to be addressed by conventional numerical approaches employing rigorous electromagnetic simulations, the neural network-based methodology presented in this work provides a promising platform for tackling computation-heavy optimization tasks with one-time computation cost.

Author contributions: S.K., J.M.S., and M.S.J conceived the ideas. S.K. performed neural network computations. J.M.S., C.P., S.L., and J.P. developed the rigorous CPS model for data creation. J.L. and S.P. analyzed the resulting OLED structures from the optimizations. S.K., D.S., and C.Y.P. conducted detailed analysis on the machine learning results. M.S.J. supervised the project. The manuscript was mainly written by S.K and M.S.J. with the contributions of all authors.

Research funding: This work was supported by LG Display and by the National Research Foundation of Korea (NRF) funded by Ministry of Science and ICT (Grants No. 2019K1A3A1A14064929, 2017R1E1A1A01074323, and 2016M3D1A1900038). This work was also supported by the BK21 FOUR Program through the NRF funded by Ministry of Education.

Conflict of interest statement: The authors declare no conflicts of interest regarding this article.

References

[1] C. W. Tang and S. A. Vanslyke, "Organic electroluminescent diodes," *Appl. Phys. Lett.*, vol. 51, no. 12, pp. 913–915, 1987.
[2] T. Sekitani, H. Nakajima, H. Maeda, et al., "Stretchable active-matrix organic light-emitting diode display using printable elastic conductors," *Nat. Mater.*, vol. 8, no. 6, pp. 494–499, 2009.
[3] M. S. White, M. Kaltenbrunner, E. D. Glowacki, et al., "Ultrathin, highly flexible and stretchable PLEDs," *Nat. Photonics*, vol. 7, no. 10, pp. 811–816, 2013.
[4] F. So, J. Kido, and P. Burrows, "Organic light-emitting devices for solid-state lighting," *MRS Bull.*, vol. 33, no. 7, pp. 663–669, 2008.
[5] H. W. Chen, J. H. Lee, B. Y. Lin, S. Chen, and S. T. Wu, "Liquid crystal display and organic light-emitting diode display: present status and future perspectives," *Light Sci. Appl.*, vol. 7, p. 17168, 2018.
[6] K. T. Kamtekar, A. P. Monkman, and M. R. Bryce, "Recent advances in white organic light-emitting materials and devices (WOLEDs)," *Adv. Mater.*, vol. 22, no. 5, pp. 572–582, 2010.
[7] J.-K. Yoon, H.-W. Park, J.-S. Son, et al., "The study of picture quality of OLED TV with WRGB OLEDs structure," *Soc. Inf. Disp.*, vol. 44, no. 1, pp. 326–329, 2013.
[8] Y. G. Huang, E. L. Hsiang, M. Y. Deng, and S. T. Wu, "Mini-LED, micro-LED and OLED displays: present status and future perspectives," *Light Sci. Appl.*, vol. 9, no. 1, p. 105, 2020.
[9] L. H. Smith, J. A. E. Wasey, and W. L. Barnes, "Light outcoupling efficiency of top-emitting organic light-emitting diodes," *Appl. Phys. Lett.*, vol. 84, no. 16, pp. 2986–2988, 2004.
[10] J. Chan, A. D. Rakic, C. Y. Kwong, et al., "Optimization of organic light emitting diode structures," *Proc. SPIE*, vol. 5277, pp. 311–319, 2004.
[11] W. G. Quirino, K. C. Teixeira, C. Legnani, et al., "Improved multilayer OLED architecture using evolutionary genetic algorithm," *Thin Solid Films*, vol. 518, no. 5, pp. 1382–1385, 2009.
[12] J. Lee, T. H. Han, M. H. Park, et al., "Synergetic electrode architecture for efficient graphene-based flexible organic light-emitting diodes," *Nat. Commun.*, vol. 7, p. 11791, 2016.
[13] C. C. Nadell, B. H. Huang, J. M. Malof, and W. J. Padilla, "Deep learning for accelerated all-dielectric metasurface design," *Opt. Express*, vol. 27, no. 20, pp. 27523–27535, 2019.
[14] Y. Kiarashinejad, S. Abdollahramezani, and A. Adibi, "Deep learning approach based on dimensionality reduction for designing electromagnetic nanostructures," *Npj Comput. Mater.*, vol. 6, no. 1, p. 12, 2020.
[15] I. Malkiel, M. Mrejen, A. Nagler, U. Arieli, L. Wolf, and H. Suchowski, "Plasmonic nanostructure design and characterization via deep learning," *Light Sci. Appl.*, vol. 7, p. 60, 2018.
[16] P. R. Wiecha and O. L. Muskens, "Deep learning meets nanophotonics: a generalized accurate predictor for near fields and far fields of arbitrary 3D nanostructures," *Nano Lett.*, vol. 20, no. 1, pp. 329–338, 2020.
[17] W. Ma, F. Cheng, and Y. M. Liu, "Deep-learning-enabled on-demand design of chiral metamaterials," *ACS Nano*, vol. 12, no. 6, pp. 6326–6334, 2018.
[18] J. Lenaerts, H. Pinson, and V. Ginis, "Artificial neural networks for inverse design of resonant nanophotonic components with oscillatory loss landscapes," *Nanophotonics*, vol. 10, no. 1, pp. 385–392, 2021.
[19] J. Peurifoy, Y. C. Shen, L. Jing, et al., "Nanophotonic particle simulation and inverse design using artificial neural networks," *Sci. Adv.*, vol. 4, no. 6, 2018, Art no. eaar4206.
[20] J. Q. Jiang, D. Sell, S. Hoyer, J. Hickey, J. J. Yang, and J. A. Fan, "Free-form diffractive metagrating design based on generative adversarial networks," *ACS Nano*, vol. 13, no. 8, pp. 8872–8878, 2019.
[21] Z. C. Liu, D. Y. Zhu, S. P. Rodrigues, K. T. Lee, and W. S. Cai, "Generative model for the inverse design of metasurfaces," *Nano Lett.*, vol. 18, no. 10, pp. 6570–6576, 2018.
[22] F. F. Wen, J. Q. Jiang, and J. A. Fan, "Robust freeform metasurface design based on progressively growing generative networks," *ACS Photonics*, vol. 7, no. 8, pp. 2098–2104, 2020.
[23] J. Q. Jiang and J. A. Fan, "Global optimization of dielectric metasurfaces using a physics-driven neural network," *Nano Lett.*, vol. 19, no. 8, pp. 5366–5372, 2019.
[24] I. Sajedian, J. Kim, and J. Rho, "Finding the optical properties of plasmonic structures by image processing using a combination of convolutional neural networks and recurrent neural networks," *Microsyst. Nanoeng.*, vol. 5, p. 27, 2019.
[25] W. Ma, F. Cheng, Y. H. Xu, Q. L. Wen, and Y. M. Liu, "Probabilistic representation and inverse design of metamaterials based on a deep generative model with semi-supervised learning strategy," *Adv. Mater.*, vol. 31, no. 35, 2019, Art no. 1901111.

[26] M. A. Bin Janai, K. L. Woon, and C. S. Chan, "Design of efficient blue phosphorescent bottom emitting light emitting diodes by machine learning approach," *Org. Electron.*, vol. 63, pp. 257–266, 2018.
[27] R. Gomez-Bombarelli, J. Aguilera-Iparraguirre, T. D. Hirzel, et al., "Design of efficient molecular organic light-emitting diodes by a high-throughput virtual screening and experimental approach," *Nat. Mater.*, vol. 15, no. 10, pp. 1120–1127, 2016.
[28] Shahnawaz, S. S. Swayamprabha, M. R. Nagar, et al., "Hole-transporting materials for organic light-emitting diodes: an overview," *J. Mater. Chem. C*, vol. 7, no. 24, pp. 7144–7158, 2019.
[29] R. R. Chance, A. Prock, and R. Silbey, "Molecular fluorescence and energy transfer near metal interfaces," *Adv. Chem. Phys.*, vol. 37, pp. 1–65, 1978.
[30] D. J. Liu, Y. X. Tan, E. Khoram, and Z. F. Yu, "Training deep neural networks for the inverse design of nanophotonic structures," *ACS Photonics*, vol. 5, no. 4, pp. 1365–1369, 2018.
[31] C. Yeung, J. M. Tsai, B. King, et al., "Multiplexed supercell metasurface design and optimization with tandem residual networks," *Nanophotonics*, vol. 10, no. 3, pp. 1133–1143, 2021.
[32] J. M. Johnson and Y. Rahmatsamii, "Genetic algorithm optimization and its application to antenna design," in *Proc. of IEEE Antennas and Propagation Society International Symposium and URSI National Radio Science Meeting*, Seattle, WA, USA, IEEE, vol. 1, 1994, pp. 326–329.
[33] K. Stanislawska, K. Krawiec, and T. Vihma, "Genetic programming for estimation of heat flux between the atmosphere and sea ice in polar regions," in *Proc. of the 2015 Annual Conf. on Genetic and Evolutionary Computation*, Madrid, Spain, Association for Computing Machinery, 2015, pp. 1279–1286.
[34] G. J. Tan, J. H. Lee, S. C. Lin, R. D. Zhu, S. H. Choi, and S. T. Wu, "Analysis and optimization on the angular color shift of RGB OLED displays," *Opt. Express*, vol. 25, no. 26, pp. 33629–33642, 2017.
[35] Y. N. Lai, C. H. Chang, P. C. Wang, and Y. H. Chu, "Highly efficient flexible organic light-emitting diodes based on a high-temperature durable mica substrate," *Org. Electron.*, vol. 75, 2019, Art no. 105442.
[36] E. Archer, S. Hillebrandt, C. Keum, et al., "Accurate efficiency measurements of organic light-emitting diodes via angle-resolved spectroscopy," *Adv. Opt. Mater.*, vol. 9, no. 1, 2021, Art no. 2000838.
[37] M. Thomschke, R. Nitsche, M. Furno, and K. Leo, "Optimized efficiency and angular emission characteristics of white top-emitting organic electroluminescent diodes," *Appl. Phys. Lett.*, vol. 94, no. 8, 2009, Art no. 083303.

Supplementary Material: The online version of this article offers supplementary material (https://doi.org/10.1515/nanoph-2021-0434).